





Topical Application of Cell-Penetrating Peptide Modified Anti-VEGF Drug Alleviated Choroidal Neovascularization in Mice

Weinan Hu , Wenting Cai , Yan Wu, Chengda Ren, Donghui Yu, Tingting Li, Tianyi Shen , Ding Xu, Jing Yu 

Department of Ophthalmology, Shanghai Tenth People's Hospital, Tongji University, Shanghai, People's Republic of China

*These authors contributed equally to this work

Correspondence: Ding Xu; Jing Yu, Email 15821885240@163.com; dryujing@aliyun.com

Background: Age-related macular degeneration (AMD) stands as the foremost cause of irreversible central vision impairment, marked by choroidal neovascularization (CNV). The prevailing clinical approach to AMD treatment relies on intravitreal injections of anti-vascular endothelial growth factor (VEGF) drugs. However, this method is encumbered by diverse complications, prompting exploration of non-invasive alternatives such as ocular administration via eye drops for anti-VEGF therapy.

Methods: Two complexes, 5-FITC-CPP-Ranibizumab (5-FCR) and 5-FITC-CPP-Conbercept (5-FCC), were synthesized by incorporating the anti-VEGF drugs Ranibizumab (RBZ) or Conbercept (CBC) with cell-penetrating peptide (CPP). Circular dichroism spectrum (CD) facilitated complexes characterization. Eye drops was utilized to address laser-induced CNV in mice. Fluorescein fundus angiography (FFA) observe the CNV lesion, while FITC-dextran and IB4 dual fluorescent staining, along with hematoxylin-eosin (HE) staining, assessed in lesion size. Tissue immunofluorescence examined CD31 and VEGF expression in choroidal/retinal pigment epithelial (RPE) tissues. Biocompatibility and biosafety of 5-FCR and 5-FCC was evaluated through histological examination of various organs or cell experiments.

Results: Both 5-FCR and 5-FCC exhibited favorable biocompatibility and safety profiles. VEGF-induced migration of Human umbilical vein endothelial cells (HUVECs) significantly decreased post-5-FCR/5-FCC treatment. Additionally, both complexes suppressed VEGF-induced tube formation in HUVECs. FFA results revealed a significant improvement in retinal exudation in mice. Histological examination unveiled the lesion areas in the 5-FCR and 5-FCC groups showed a significant reduction compared to the control group. Similar outcomes were observed in histological sections of the RPE-choroid-sclera flat mounts.

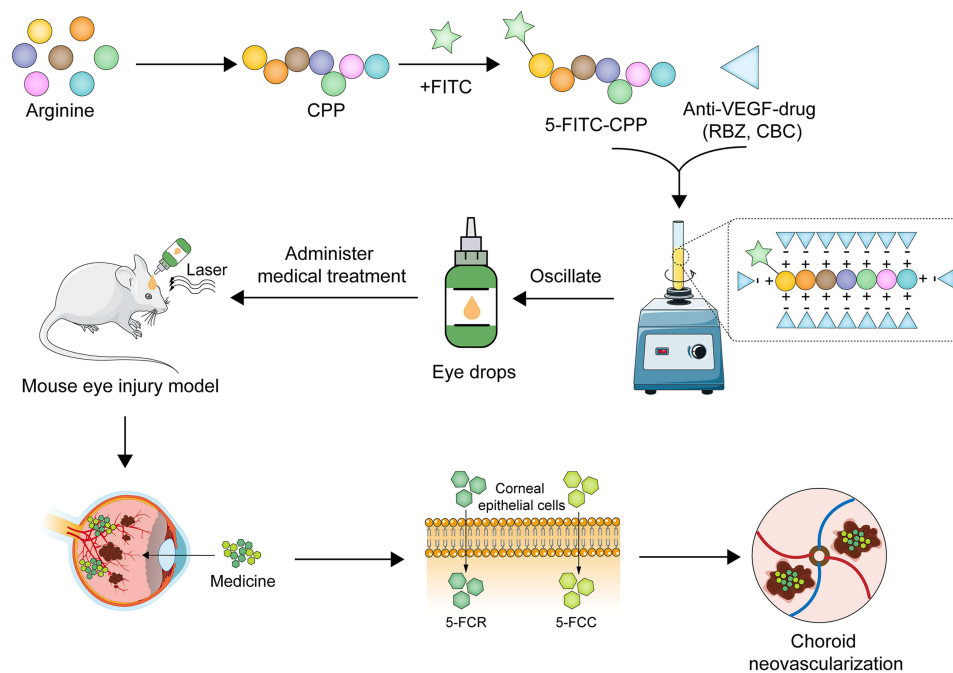
Conclusion: In this study, utilizing the properties of CPP and two anti-VEGF drugs, we successfully synthesized two complexes, 5-FCR and 5-FCC, through a straightforward approach. Effectively delivering the anti-VEGF drugs to the target area in a non-invasive manner, suppressing the progression of laser-induced CNV. This offers a novel approach for the treatment of wet AMD.

Keywords: age-related macular degeneration, choroidal neovascularization, cell-penetrating peptide, ranibizumab, conbercept, drug delivery

Introduction

Age-related macular degeneration (AMD) ranks as the third leading cause of severe and irreversible visual impairment globally.¹ According to statistics, approximately 200 million individuals were affected by AMD worldwide in 2020, and this number is projected to exceed 400 million by 2040.² Neovascular AMD (nAMD), also known as wet AMD, is characterized by the development of choroidal neovascularization, leading to subretinal fluid, intraretinal fluid, and retinal hemorrhage.^{3,4} Ultimately, this progression results in the formation of subretinal fibrotic scar tissue, causing significant visual impairment and even blindness.⁵

Graphical Abstract



Vascular endothelial growth factor (VEGF) plays a crucial role in the occurrence and development of choroidal neovascularization (CNV).⁶ VEGF is often derived from endothelial cells, Müller cells, and RPE cells.⁷ It stimulates the growth of vascular endothelial cells from arterial, venous, and lymphatic sources.⁸ Under normal physiological conditions, pro-angiogenic factors and anti-angiogenic factors are in dynamic equilibrium. However, under pathological conditions, hypoxia-inducible factors (HIFs) induced by oxygen deficiency leading to an upregulation of pro-angiogenic factors such as VEGF.^{9,10} This, in turn, results in abnormal neovascular growth.

Therapeutic strategies for nAMD encompass laser photocoagulation, photodynamic therapy (PDT), anti-VEGF treatment, and combination therapies.¹¹ Presently, the most widely employed clinical approach involves intravitreal injection of anti-VEGF drugs into the vitreous cavity, which blocks the occurrence and development of CNV.¹² Ranibizumab (RBZ) and conbercept (CBC) are currently the most commonly used anti-VEGF drugs for the treatment of AMD.^{13,14} Among these, RBZ is a recombinant humanized Fab fragment derived from a monoclonal antibody, which can bind to all the biologically active VEGF isoforms with high affinity. Importantly, it effectively prevents CNV development and controls neovascular leakage.¹⁵ In addition, CBC, a recombinant fusion protein with high affinity to all VEGF isoforms and placental growth factor (PlGF), was developed and approved in China in 2013 for the treatment of wet AMD, with definite clinical efficacy.¹⁶ Although many studies^{17–19} have emphasized that intravitreal injection of anti-VEGF drugs has a good effect on the treatment of CNV, it is an invasive procedure that suffers from some injection-related complications, such as intraocular infection, retinal detachment, and cataracts, which could lead to severe visual impairment.^{20–22} In addition, the therapy requires multiple repeated injections, and the drugs are expensive, placing a financial strain on patients. Therefore, developing an effective, safe and non-invasive drug delivery method is an urgent requisite.

The use of topical eye drops is a commonly employed therapeutic method in ophthalmology, offering the advantages of convenience in administration and the ability for self-administration over an extended period. This approach demonstrates outstanding efficacy in the treatment of ocular surface diseases.²³ Additionally, eye drops significantly reduce the incidence of systemic reactions, boasting a high safety profile and serving as a suitable alternative to intravitreal injections. Previous research indicates that novel eye drop formulations, synthesized using advanced molecular materials such as Amination-mediated nano eye drops²⁴ and multifunctional glutathione-dependent hydrogel,²⁵ exhibit enhanced corneal permeability and

increased drug bioavailability. Enabling a faster and more sustained treatment of glaucoma. However, challenges persist in utilizing local eye drops for the treatment of retinal diseases due to the unique structure of the eyeball and the presence of the blood-ocular barrier.²⁶ Consequently, there is a need for a safe carrier capable of transporting drugs through ocular structures to reach the affected site.

Cell-penetrating peptides (CPPs) are a family of peptides consisting of 30 or fewer amino acid structures.²⁷ These peptides can pass through the mammalian and plant cell membranes without interaction with receptors, exhibit low cytotoxicity, and can bind with the cargo in a covalent or non-covalent manner to promote the cellular internalization of the cargo.^{28,29} Therefore, using CPPs as a drug carrier for clinical treatment has become one of the research hotspots.

In this study, the desired CPP carrier was first synthesized, modified with a fluorophore 5-FITC, and then conjugated with anti-VEGF drugs to construct complete finished complexes 5-FITC-CPP-Ranibizumab (5-FCR) and 5-FITC-CPP-Conbercept (5-FCC). In addition, the biosafety of the two finished particles was verified through cell and animal experiments, and then the therapeutic effect of the eye drops was verified in a laser-induced mouse CNV model. This study utilizes the advantages of non-viral vectors to non-invasively deliver drugs to the lesion site, providing an alternative strategy for CNV treatment.

Materials and Methods

Materials

The following reagents were used in this study: Fmoc-Arg(pbf)-OH (Chengdu Chengnuo New Technology Co., Ltd, Sichuan, China), Fmoc-ACP-OH (Beijing Bailingwei Technology Co., Ltd, Beijing, China), 5-FITC (Shanghai Yuanye Biotechnology Co., Ltd, Shanghai, China), RBZ (Novartis Pharma Schweiz AG, Risch, Switzerland), CBC (Chengdu Kanghong Biotechnology Co., Ltd, Sichuan, China), Human retinal pigment epithelium cell line (ARPE-19) (iCell Bioscience Inc, Shanghai, China), Human umbilical vein endothelial cells (HUVECs) (ScienCell, California, USA), DMEM/F12 medium (Gibco, Risch, Switzerland), Fetal bovine serum (Gibco, New York, USA), Penicillin/streptomycin (Gibco), Cell Counting Kit-8 (CCK-8) (Shanghai Yisheng Biotechnology Co., Ltd, Shanghai, China), Sodium pentobarbital (Shanghai Beyotime Biotechnology Co., Ltd, Technology Co., Ltd, Shanghai, China), Proparacaine hydrochloride eye drops (Alcon, Geneva, Switzerland).

Synthesis of 5-FITC-CPP

2-Chlorotrityl chloride resin was combined with 15 mL/g of dichloromethane (DCM) for 30 min. Fmoc-Arg(pbf)-OH (arginine) was introduced in a three-fold molar excess, dissolved in *N,N*-dimethylformamide (DMF), and mixed with a ten-fold molar excess of diisopropylethylamine (DIEA) on the resin for 60 min. Subsequent resin blocking with methanol followed. The DMF in the reaction tube was removed, and a 20% piperidine DMF solution (15mL/g) was added for deprotection, and the process was iterated to reveal exposed amino acid sites. Detection of these sites was accomplished by introducing 2-Chlorotrityl chloride resin and observing dark blue binding sites using the Kaiser detection reagent after heating. Condensation involved washing the resin, adding excess amino acid, *N,N,N',N'*-Tetramethyl-O-(1H-benzotriazol-1-yl)uronium hexafluorophosphate (HBTU), and DIEA for a 30-minute reaction, followed by site detection. Subsequently, peptide cleavage was achieved by washing with DMF and DCM and treating with a cleavage solution (TFA:water:EDT:TIS = 95:1:2:2) for 120 min. Purification was carried out by concentrating the cleavage solution, washing with ether, and collecting peptides through high-performance liquid chromatography (HPLC). The resulting polypeptide solution was lyophilized to yield a faint yellow lyophilized powder or crystallization (302 mg, 18% yield, 98.24% purity) which was identified by electrospray ionization mass spectrometry (ESI - MS).

Synthesis of 5-FCR and 5-FCC

Prior to use, an appropriate amount of the undiluted solution of RBZ or CBC at a concentration of 10 mg/mL is obtained. The solution is then diluted to the desired concentration using a phosphate-buffered saline (PBS) solution. Subsequently, a suitable quantity of 5-FITC-CPP lyophilized powder or crystallization is added to the solution, and the mixture is vortexed for 10s using a vortex mixer. The solution is then filtered, collected, and stored at 4 °C until further use.

Characterization

Hydrodynamic Size and Surface Potential

For the determination of dynamic light scattering (DLS) and zeta potential (ZP), 5 mg of 5-FITC-CPP powder was dissolved in 1 mL of PBS solution. Additionally, 1 mL each of the solutions for 5-FCR (5 mg 5-FITC-CPP + 1.8 mg/mL RBZ) and 5-FCC (5 mg 5-FITC-CPP + 1.8 mg/mL CBC) were prepared. The DLS and ZP of the materials was measured using a Malvern Zetasizer (ZEN3600 Nano ZS, Worcestershire, UK).

Circular Dichroism (CD) Analysis

CD was employed to characterize the concentration-dependent impact on the formation of complexes involving 5-FITC-CPP with RBZ or CBC. CD spectra were acquired using a Jasco J-815 spectropolarimeter (Jasco UK, Great Dunmow, UK) in 10-mm pathlength quartz cuvettes. The stock solution of RBZ or CBC (1.8 mg/mL) was read at 200 to 300 nm. To initiate complex formation, an appropriate quantity of 5-FITC-CPP was introduced into the RBZ and CBC solutions. Then, the ellipticity values were recorded.

Cell Counting Kit (CCK)-8 Detection of Cell Viability

ARPE-19 cells were seeded at a concentration of 5000 cells/well in three 96-well plates, incubated overnight at 37°C. After cell adhesion, different concentrations of 5-FITC-CPP (1.5, 3.5, 7.5, 15, 35, 75, 150, 350, 750, 1500 µg/mL), 5-FCR (150 µg/mL 5-FITC-CPP + 1, 5, 10, 50, 100, 200, 500 µg/mL RBZ), and 5-FCC (150 µg/mL 5-FITC-CPP + 1, 5, 10, 50, 100, 200, 500 µg/mL CBC) were added to the experimental wells. The cells were then incubated at 37°C for 24 h. Subsequently, 10 µL of CCK-8 reagent was added to each well, and the plates were incubated in the dark for 2 h. The absorbance at 450 nm was measured using a microplate reader. The same treatment was applied to HUVECs.

Cellular Uptake Assays

ARPE-19 cells were cultured in a 12-well plate (10^5 cells/well) until reaching confluence. Different concentrations of 5-FITC-CPP (150, 350, 750 µg/mL) were added, followed by a 1 h incubation. Subsequently, cells were washed three times with PBS, and Hoechst-33,342 live cell staining solution (1:1000) was added, with a 10 min incubation. After another three washes with PBS, images were captured under a fluorescence microscope.

Tube Formation Assay

Matrigel was applied to 96-well plates and allowed to solidify at 37°C for 30 min. Then, each well was seeded with 100 µL of HUVECs (5×10^3 /well), which were subjected to the aforementioned treatment. After 6 h of incubation, the cell images were captured using a light microscope.

Wound-Healing Assay

HUVECs were seeded in 6-well plates at a density of 1×10^5 cells per well. Wounds were introduced in the middle of the cell monolayer when it reached 80% confluence using a 200 µL pipette tip. The initial images were captured at 0 h, and the cells were subjected to the previously described treatment. The closure of the wound was evaluated after 24 and 48 h of incubation by measuring the widths of the scratches, and the migration rates were calculated using the formula (distance/scratch width) \times 100%. The experiments were independently repeated three times.

Animals

C57BL/6 mice (SLAC Laboratory Animal Corporation, Shanghai, China) were bred at the Animal Experiment Center of Tongji University (Shanghai, China). Mice were housed with a 12 h light/12 h dark cycle and provided ad libitum access to water and standard laboratory feed. All animal procedures adhered to the Association for Research in Vision and Ophthalmology (ARVO) guidelines for ethical use in ophthalmology and vision research. The study protocol received approval from the Animal Use and Care Committee of Tongji University (approval number: wyd2017-0056f). Only male mice were used in the study.

Establishment of the Mouse CNV Model

C57BL/6 mice weighing 25 ± 3 g were intraperitoneally injected with 40 mg/kg of 1% sodium pentobarbital for general anesthesia. Tropicamide eye drops induced pupil dilation, and proparacaine hydrochloride eye drops provided local anesthesia. After completing anesthesia, mice eyeballs were fully exposed. A glass slide was applied with ofloxacin eye ointment and positioned as a contact lens in the corner of the mice eyes. Using a laser photocoagulation microscope with the following laser settings: wavelength: 532-nm, power: 160 mV, duration: 0.08 s, spot size: 50 μ m. Laser shots were applied between every two retinal vessels, with 1–2 points per shot. Successful modeling criteria included the presence of fissure bubbles or slight hemorrhage at the photocoagulation site observed under a slit-lamp microscope.

Animal Grouping

The animals were grouped and treated as follows: (1) Control group (n=10): Mice without laser photocoagulation; (2) PBS group (n=10): Mice underwent laser photocoagulation, followed by the administration of 25 μ L of 1 \times PBS eye drops (once every 12 h); (3) 5-FITC-CPP group (n=10): Mice, after laser photocoagulation, received 25 μ L of 5-FITC-CPP (5 mg/mL) eye drops (once every 12 h); (4) RBZ treatment group (n=50) consisted of the following subgroups: (i) 5-FCR eye drop subgroup (n=30): following laser photocoagulation, mice received 25 μ L of 5-FCR eye drops (once every 12 h). The concentrations were as follows: low concentration: 5 mg/mL CPP+0.072 mg/mL RBZ; medium concentration: 5 mg/mL CPP+0.36 mg/mL RBZ; high concentration: 5 mg/mL CPP+1.8 mg/mL RBZ; (ii) RBZ-alone eye drop subgroup (n=10): after laser photocoagulation, mice received 25 μ L of 10 mg/mL RBZ-alone eye drops (once every 12 h). (iii) RBZ injection subgroup (n=10): following laser photocoagulation, 1 μ L of 10 mg/mL RBZ was injected into the vitreous cavity of mice; (5) CBC treatment group (n=50) included the following subgroups: (i) 5-FCC eye drop subgroup (n=30): after laser photocoagulation, mice received 25 μ L of 5-FCC eye drops (once every 12 h). The concentrations were as follows: low concentration: 5 mg/mL CPP+0.072 mg/mL CBC; medium concentration: 5 mg/mL CPP+0.36 mg/mL CBC; high concentration: 5 mg/mL CPP+1.8 mg/mL CBC; (ii) CBC-alone eye drop subgroup (n=10): following laser photocoagulation, mice received 25 μ L of 10 mg/mL CBC-alone eye drops (once every 12 h). (iii) CBC injection subgroup (n=10): after laser photocoagulation, 1 μ L of 10 mg/mL CBC was injected into the vitreous cavity of mice.

Fluorescein Fundus Angiography (FFA)

After successful model induction, mice underwent the specified interventions as described above. FFA were conducted at 7, 14, 28 days post-intervention. Mice were anesthetized by intraperitoneal injection of 40 mg/kg 1% sodium pentobarbital. Following anesthesia, compound tropicamide eye drops were used for pupil dilation, and proparacaine hydrochloride eye drops provided topical anesthesia. Subsequently, 2 mL of 1% sodium fluorescein solution was injected into the mice's abdominal cavity, and FFA was performed to capture angiographic images.

Measurement of the CNV Area

Mice from each intervention group, following a 28-day treatment period, were anesthetized, and 20 mL of 1X PBS solution was rapidly injected into the left ventricle. After perfusion, 0.2 mL of FITC-Dextran solution (25 mg/mL) was injected through the same site. Following a 3–5 min interval, 20 mL of 4% paraformaldehyde solution was slowly injected for fixation. During the injection process, slight yellowish discoloration around the mouse's nose and tail, as well as mild tremors and tail rotation, were observed.

The mice eyeballs were extracted and immersed in 4% paraformaldehyde solution for fixation for 2 h. Subsequently, excess connective tissue, cornea, lens, and vitreous were removed from the eyeballs. The retina and nerve epithelial layer were gently separated and removed, and the remaining tissue was cut into four quadrants. With the sclera facing down, the tissue was laid flat on a glass slide. After incubating with IB4 (1:1000) for 20 min, the tissues were rinsed three times with 1X PBS solution. Fluorescent microscopy was then used to document the CNV size on the slide, and the area of CNV was measured using ImageJ software (National Institutes of Health, Bethesda, MD, USA).

HE Staining

After a 28-day intervention, the eyeballs from each experimental group were extracted and immersed in eyeball fixative for 24 h. The eye tissues underwent dehydration in graded ethanol, paraffin embedding, routine sectioning at a 4 μm thickness, HE staining, and mounting with neutral gum. The ImageJ software was employed to calculate the area of CNV lesions.

Immunofluorescence Staining of Eyeballs

The mice eyeballs slices were placed in EDTA antigen retrieval solution and subjected to antigen retrieval in a 95°C water bath for 20 min. Subsequently, they were incubated with rabbit anti-VEGF antibody (1:50, Proteintech, Chicago, IL, USA) and mouse anti-CD31 antibody (1:50, Cell Signaling Technology, Danvers, MA, USA) overnight at 4°C in the dark. Next, the slices were incubated in the dark for 30 min with Fluorescent secondary antibody. After counterstaining the cell nuclei with DAPI (Biotium, Inc., Shanghai, China), adding an anti-fluorescence quencher, the specimens were sealed, and images were captured under a fluorescence microscope.

Biocompatibility in vivo

HE Staining

After 28 days of intervention in mice according to the above grouping, the mice were sacrificed, and the organs including brain, heart, liver, spleen, lung and kidney were extracted and fixed in 4% paraformaldehyde. The organs were embedded, sectioned, and stained with HE according to the protocol. The CNV area was imaged by a light microscope.

Corneal Fluorescein Sodium Staining

Following the 28-day intervention, mice were intraperitoneally anesthetized with 1% sodium pentobarbital, and fluorescein sodium dye was uniformly applied to the corneal surface. Subsequently, corneal fluorescein staining images were acquired using a handheld slit lamp microscope with the following settings: 10x eyepiece, 2x objective, 5 mm slit width, 5 mm beam diameter, and cobalt blue light.

Statistical Analysis

In this investigation, statistical analyses were conducted using SPSS 20.0 software and Graph Pad Prism version 8. A one-way analysis of variance (ANOVA) was employed to assess variations across multiple groups. Significance was determined at a threshold of 0.05, with P-values below this threshold considered indicative of statistical significance.

Results

Synthesis and Characterization of 5-FITC-CPP, 5-FCR, and 5-FCC

In this study, we synthesized a penetrating peptide through a condensation reaction using arginine and simultaneously linked it to the 5-FITC fluorescent group, resulting in the final product, 5-FITC-CPP. In the solid state, 5-FITC-CPP appears as a light-yellow lyophilized powder or crystalline substance, with a purity of 98.24% (Figure S1). Upon dissolution, it forms a clear light-yellow solution (Figure S2A and B1–2). Due to the positively charged nature of the carrier, it can form non-covalent linkages with the negatively charged RBZ and CBC, forming the complexes 5-FCR and 5-FCC (Figure S2B3–4). We characterized them using various methods. The formation of complexes led to larger hydrodynamic sizes for 5-FCR and 5-FCC compared to 5-FITC-CPP (Figure 1A). Due to the mutual cancellation of positive and negative charges, Zeta potentials of 5-FITC-CPP, 5-FCR, and 5-FCC were 12.50 ± 0.38 , 5.73 ± 0.71 , and 0.68 ± 0.44 mV (Figure 1B), respectively. The decrease in surface potential of 5-FCR and 5-FCC also confirmed the formation of the complexes.

Meanwhile, we utilized CD to monitor the formation of two complexes. The spectrum peak of 0.36 mg/mL RBZ at 212-nm was -6.74 mdeg. Upon adding 150 μg CPP to RBZ (1 mL), this peak changed to -13.50 mdeg, and with 300 μg CPP, it further changed to -13.72 mdeg. The addition of 500 μg CPP resulted changed to -13.99 mdeg, indicating the formation of complexes between CPP and RBZ. Furthermore, the relative concentration of CPP increased to above 150 μg without significantly altering the complex structure. (Figure 1C) When 150 μg CPP was added to 0.36mg/mL CBC

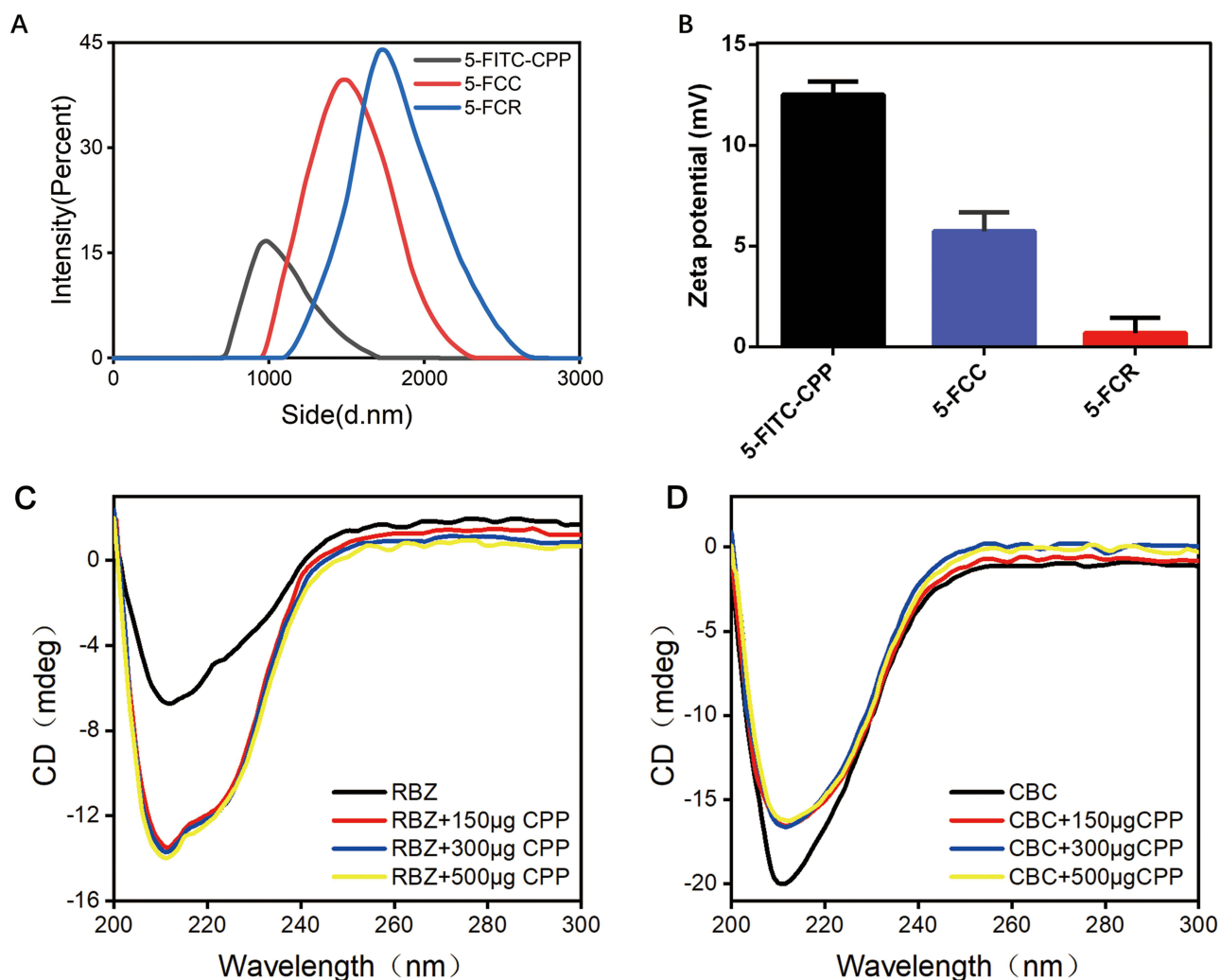


Figure 1 Synthesis and characterization of 5-FITC-CPP, 5-FCR, and 5-FCC. (A) mean particle size of 5-FITC-CPP, 5-FCR, 5-FCC. (B) Zeta surface potential of 5-FITC-CPP, 5-FCR, 5-FCC. (C) CD data of RBZ with increasing amounts of CPP in the complex. (D) CD data of CBC with increasing amounts of CPP in the complex.

(1 mL), the peak shifted from -19.99 at 211 nm to -16.53 mdeg (Figure 1D). As CPP concentration increased, there was no substantial change in the peak value, exhibiting results similar to the RBZ group.

Biocompatibility of 5-FITC-CPP

The results indicated that there were no statistically significant differences in cell viability between the CPP intervention groups at concentrations of 1.5, 3.5, 7.5, 15, 35, 75, 150, 350, 750, and 1500 $\mu\text{g/mL}$, as compared to the non-intervention group ($P > 0.05$) (Figure 2A and B). Additionally, ARPE-19 cells and HUVECs were intervened with varying concentrations of 5-FCC and 5-FCR. After 24 h of intervention, no significant reduction in cell viability was observed compared to the control group for both cell types (Figure 2C and D). These findings demonstrate the sufficient biocompatibility of 5-FITC-CPP, 5-FCR, and 5-FCC, supporting their use in subsequent experiments.

5-FITC-CPP Could Be Internalized by ARPE-19 Cells

As shown in Figure 3, incubation of 5-FITC-CPP to the cells, observation under fluorescence microscopy revealed a cytoplasm filled with green fluorescence. With an increase in the concentration of 5-FITC-CPP, the intensity of green fluorescence enhanced.

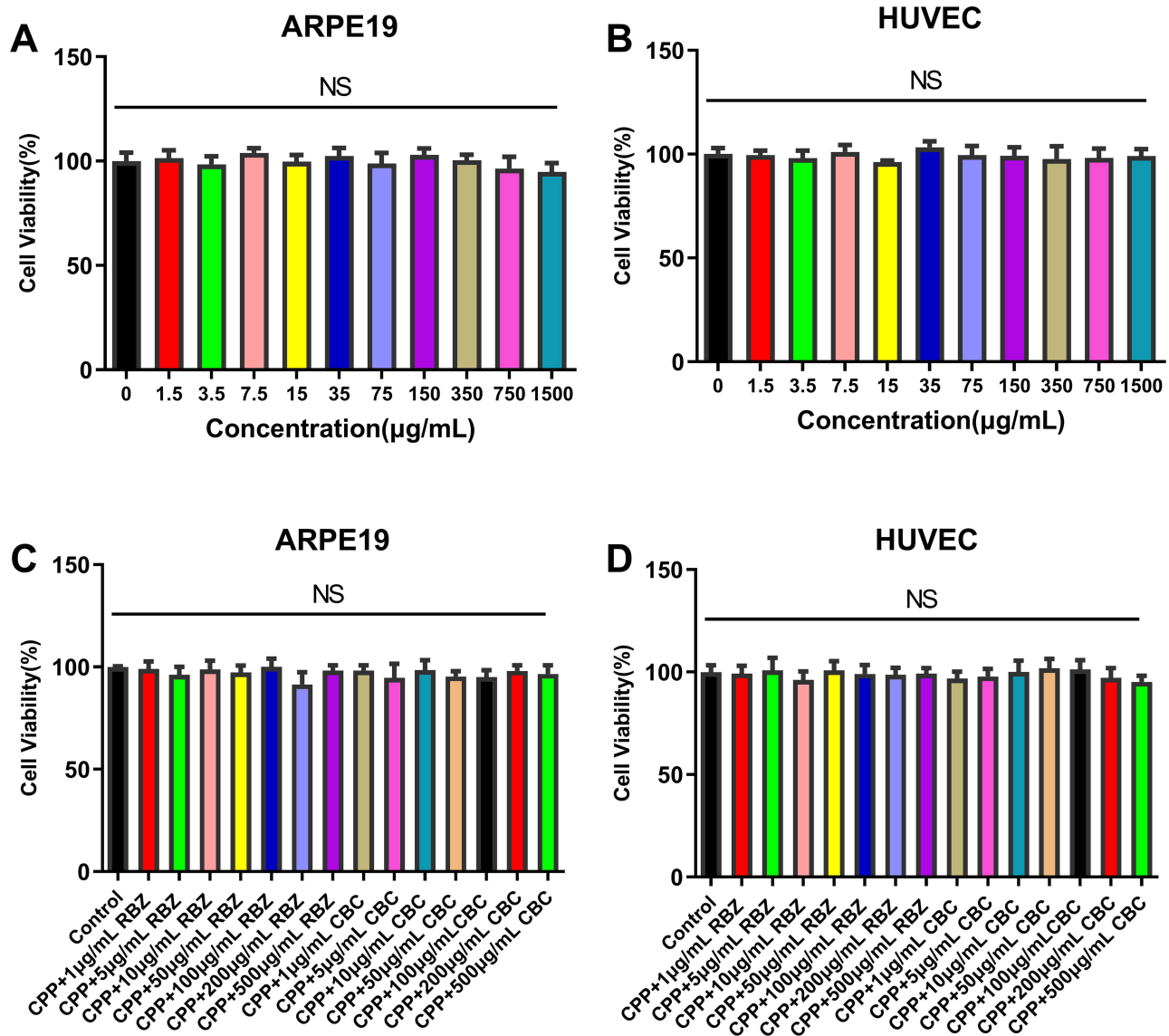


Figure 2 Cell viability effects of 5-FITC-CPP, 5-FCR, and 5-FCC on ARPE-19 cells and HUVECs were analyzed using the CCK-8 assay. (A) The activity of ARPE-19 cells under the intervention of different concentrations of 5-FITC-CPP. (B) The activity of HUVECs under the intervention of different concentrations of 5-FITC-CPP. (C) The activity of ARPE-19 cells under the intervention of different concentrations of 5-FCR and 5-FCC. (D) The activity of HUVECs under the intervention of different concentrations of 5-FCR and 5-FCC. NS: no significance.

5-FCR and 5-FCC Attenuate VEGF-Induced HUVECs Migration and Tube Formation

Wound-healing assays were performed, measuring widths at 0 h, 24 h, and 48 h as illustrated in Figure 4. Migration rates were calculated as $(24\text{ h}-0\text{ h})/0\text{ h}$ and $(48\text{ h}-0\text{ h})/0\text{ h}$. VEGF-induced HUVECs demonstrated significantly higher migration rates compared to untreated cells at 24 h and 48 h ($**p < 0.01$, $***p < 0.001$ and $****p < 0.0001$, respectively). At 24 h, the migration rates for the seven groups were 0.31 ± 0.01 , 0.56 ± 0.04 , 0.52 ± 0.02 , 0.41 ± 0.01 , 0.36 ± 0.03 , 0.21 ± 0.07 , and 0.21 ± 0.04 . Following VEGF stimulation, migration rates decreased from 0.86 ± 0.04 to $0.72 \pm 0.02/0.72 \pm 0.02$ and $0.58 \pm 0.04/0.59 \pm 0.04$ after 5-FCR/5-FCC treatment at low concentration (150 $\mu\text{g/mL}$ 5-FITC-CPP + 10 $\mu\text{g/mL}$ RBZ/CBC) and high concentration (150 $\mu\text{g/mL}$ 5-FITC-CPP + 100 $\mu\text{g/mL}$ RBZ/CBC), respectively.

Tube formation assay was employed to assess the ability of seven groups of cells to form lumens (Figure 5A). The number of nodes, junctions, segments and relative tube length for each group were calculated and analyzed. The results are presented in Figure 5B. The numbers of nodes for these seven groups were: 165.00 ± 9.42 , 314.33 ± 8.38 , 267.00 ± 22.55 , 209.67 ± 31.79 ,

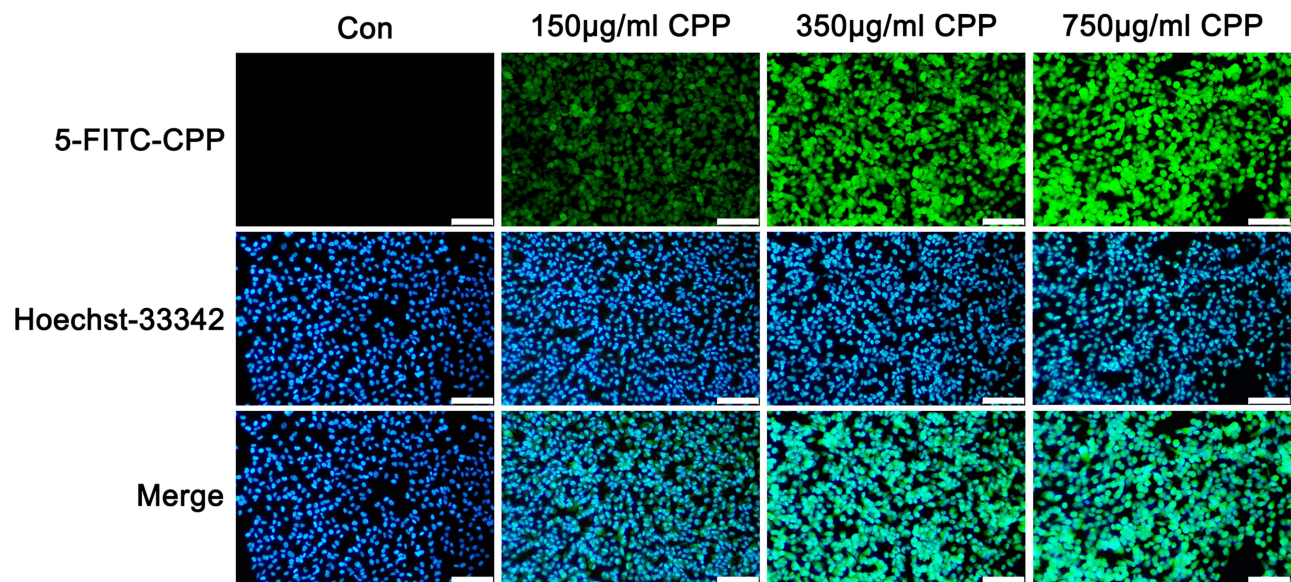


Figure 3 5-FITC was delivered by CPP to ARPE-19 cells. Scale bar: 100 µm.

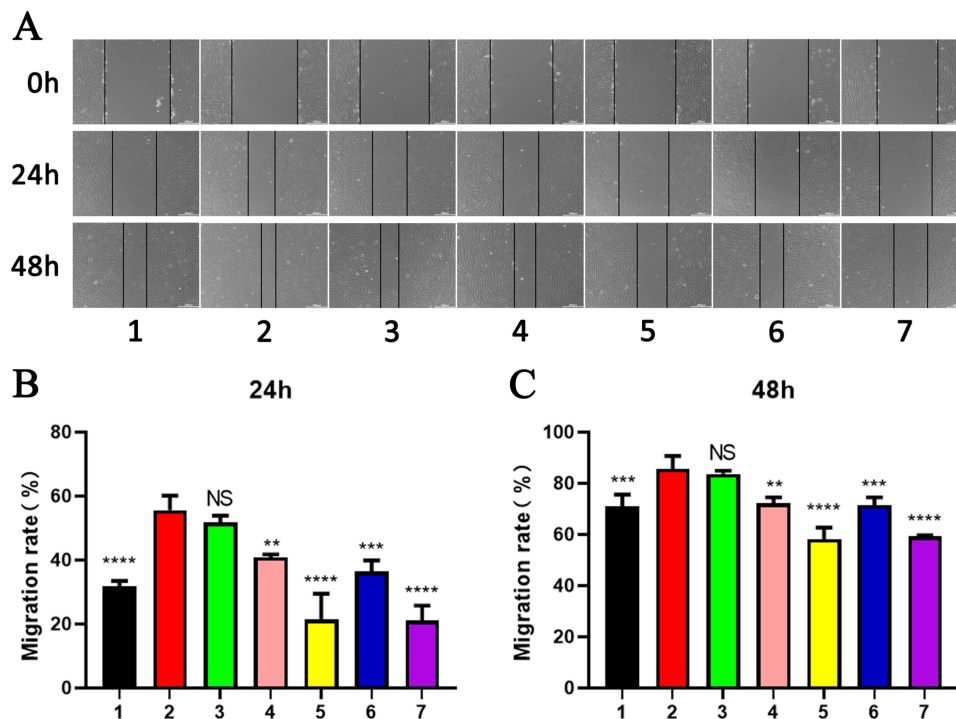


Figure 4 5-FCR or 5-FCC attenuated VEGF-induced migration of HUVECs, which was measured by wound-healing assay. (A) After treatment with 20 ng/mL of VEGF with or without 5-FCR or 5-FCC for 24h and 48 h, the migration of HUVECs with different treatments were detected via wound-healing assay analysis. Scale bar: 200 µm. Migrated cells at 24 h (B) and 48 h (C) were quantified by counting three random vision fields under a microscope. Group 1: control, Group 2: 20 ng VEGF treatment, Group 3: 20 ng VEGF with 150 µg/mL CPP treatment, Group 4: 20 ng VEGF with 150 µg/mL CPP+10 µg/mL RBZ treatment, Group 5: 20ng VEGF with 150 µg/mL CPP+100 µg/mL RBZ treatment, Group 6: 20ng VEGF with 150 µg/mL CPP+100 µg/mL CBC treatment, Group 7:20ng VEGF with 150 µg/mL CPP+100 µg/mL CBC treatment. **P<0.01, ***P<0.001, **** P<0.0001.

Abbreviation: NS, no significance.

224.67 ± 12.39, 133.67 ± 36.12, and 135.33 ± 17.63, respectively. The junction numbers were: 52.00 ± 1.41, 93.33 ± 2.87, 78.33 ± 4.50, 59.33 ± 7.93, 66.00 ± 3.74, 39.67 ± 11.67, and 39.67 ± 6.60, respectively. The segment numbers were: 65.67 ± 2.05, 128.67 ± 6.02, 103.00 ± 7.12, 78.67 ± 12.50, 82.33 ± 11.26, 49.33 ± 16.13, and 50.67 ± 7.59, respectively. Furthermore, after

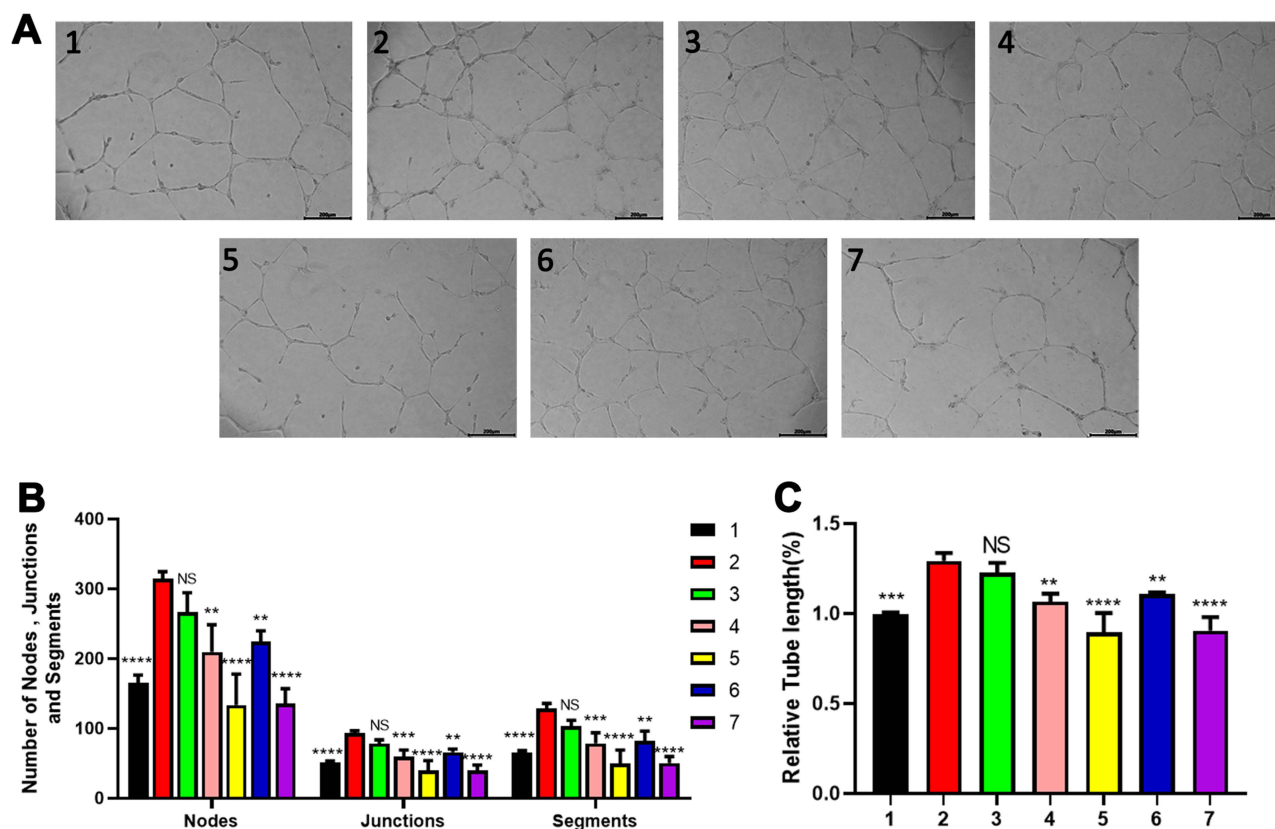


Figure 5 5-FCR or 5-FCC attenuated VEGF-induced HUVECs tube formation. (A) The tube formation was stimulated by VEGF, and inhibited by 5-FCR/5-FCC incubation. Scale bar: 200 μm (B) The numbers of nodes, junctions and segments were quantified by imageJ software. (C) The relative tube length (%) was quantified by imageJ software. Group 1: control, Group 2: 20 ng VEGF treatment, Group 3: 20 ng VEGF with 150 μg/mL CPP treatment, Group 4: 20 ng VEGF with 150 μg/mL CPP+10 μg/mL RBZ treatment, Group 5: 20ng VEGF with 150 μg/mL CPP+100 μg/mL RBZ treatment, Group 6: 20ng VEGF with 150 μg/mL CPP+10 μg/mL CBC treatment, Group 7:20ng VEGF with 150 μg/mL CPP+100 μg/mL CBC treatment. ** $P < 0.01$, *** $P < 0.001$, **** $P < 0.0001$. Abbreviation: NS, no significance.

VEGF stimulation, the relative tube length increased to 1.29 ± 0.04 . However, at a drug concentration of 100 μg/mL, 5-FCR/5-FCC treatment led to a decrease in relative tube length to 0.90 ± 0.09 and 0.90 ± 0.06 , respectively (Figure 5C).

5-FCR and 5-FCC Eye Drops Have a Significant Curative Effect on CNV

FFA results revealed that, compared to the PBS and 5-FITC-CPP groups, the 5-FCR and 5-FCC eye drop groups exhibited a significant reduction in fluorescence leakage area and a marked decrease in fluorescence intensity at 28 days. The high concentration of both 5-FCR and 5-FCC showed the most pronounced effects, comparable to the outcomes observed in the ranibizumab (RBZ) and bevacizumab (CBC) injection groups. In contrast, the RBZ-Alone and CBC-Alone eye drop groups showed no apparent therapeutic effects, as large areas of bright fluorescence leakage were still evident (Figure 6).

Following HE staining of CNV lesions, the results indicated a significant reduction in lesion area after treatment with three concentrations of 5-FCR and 5-FCC eye drops compared to the control group. All results were statistically significant (** $p < 0.01$, *** $p < 0.001$). Similar therapeutic effects were observed in the RBZ and CBC injection groups. However, the RBZ/CBC-Alone eye drop groups exhibited CNV lesion areas similar to those of the control group (Figure 7).

As illustrated in Figure 8, at 28 days post-intervention, mice hearts were perfused with FITC-dextran for staining. Eyes were collected to prepare RPE-choroid-sclera flat mounts, and double-fluorescent staining for CNV lesions was performed using IB4 antibody. Quantitative measurement of CNV areas in each group revealed that the CNV lesion area in the PBS eye drop group was $189,744.16 \pm 14,192.60 \mu\text{m}^2$, while the vehicle-only eye drop group exhibited a CNV area of $180,832.05 \pm 17,211.90 \mu\text{m}^2$.

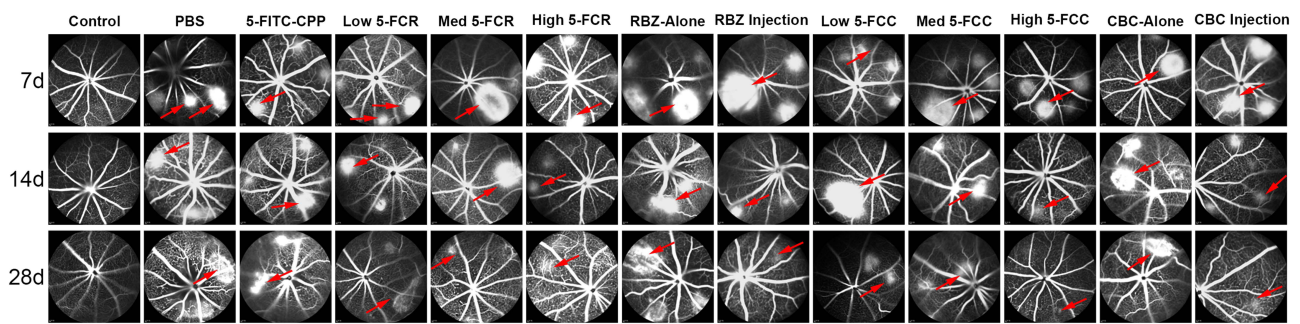


Figure 6 FAA was performed to observe the CNV lesion. Fluorescein leakage was marked by red arrow.

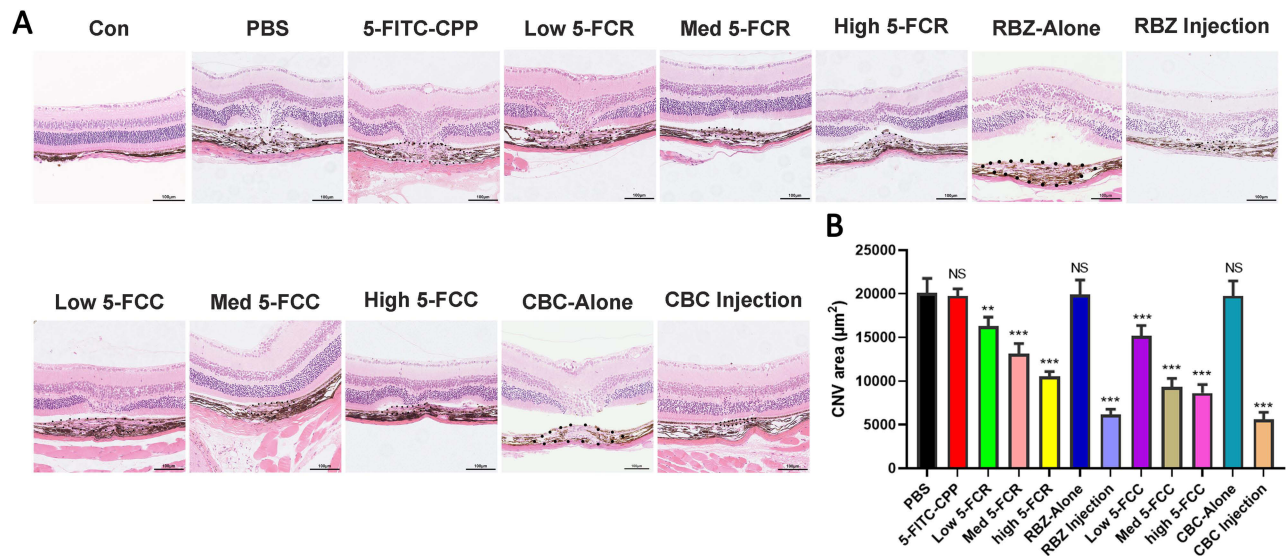


Figure 7 The CNV areas were stained and measured by HE assays. (A) The retina and choroid were examined using HE staining to visualize their structure. The presence of black spots indicated the areas of CNV. Scale bar: 100 μm . (B) The CNV length, thickness and areas were quantified in HE staining via ImageJ software. ** $P < 0.01$, *** $P < 0.001$.

Abbreviation: NS, no significance.

The CNV areas in the high-concentration 5-FCR and 5-FCC groups were significantly reduced compared to both control groups, measuring $72,674.43 \pm 6622.16 \mu\text{m}^2$ and $50,929.17 \pm 8094.10 \mu\text{m}^2$, respectively (** $p < 0.001$). Similar reductions were observed in the RBZ and CBC injection groups, with CNV areas decreasing to $35,301.42 \pm 5807.91 \mu\text{m}^2$ and $35,133.61 \pm 5188.30 \mu\text{m}^2$ (** $p < 0.001$), respectively. However, the RBZ/CBC-Alone eye drop groups showed no change compared to the control group, with CNV areas remaining at $185,910.96 \pm 18,071.54 \mu\text{m}^2$ and $191,957.54 \pm 17,007.74 \mu\text{m}^2$ ($p > 0.05$).

Fluorescent staining of CD31 and VEGF, as depicted in the aforementioned experiments, revealed similar outcomes. The 5-FCR and 5-FCC eye drop groups exhibited suppression of CNV formation by intervening in the expression of CD31 and VEGF. Similar results were observed in the RBZ and CBC injection groups. In contrast, the standalone drug eye-drop groups exhibited strong expressions of CD31 and VEGF (Figure 9).

Safety Assessment of 5-FCR and 5-FCC Eye Drops on Ocular Tissues and Internal Organs

To evaluate the safety of 5-FCR and 5-FCC eye drops on the cornea, fluorescein sodium staining was performed on the corneas of mice in each group on the 7th, 14th, and 28th day of the intervention. The corneas were examined for any signs of damage. Cobalt blue light from a slit lamp was used for corneal inspection, and no significant abnormalities were observed. Corneal staining images were captured on the 28th day. No apparent corneal damage was observed in the

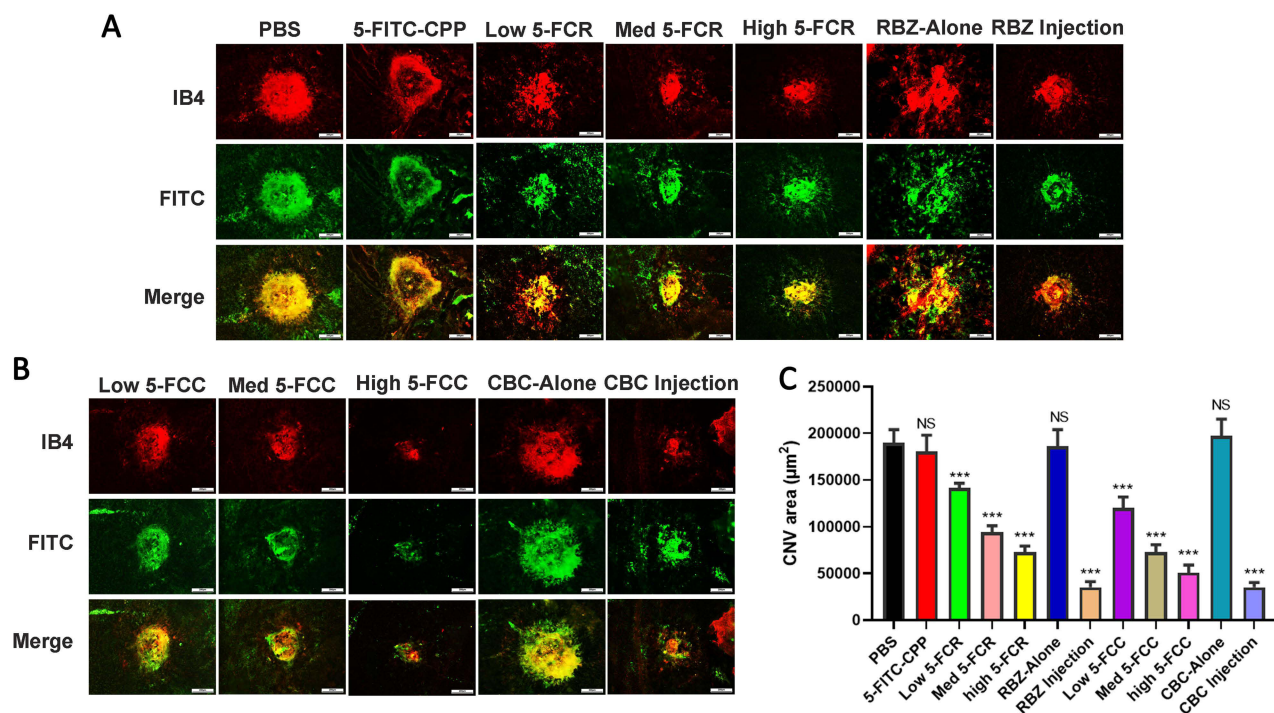


Figure 8 RPE-choroid-sclera flat mounts were prepared by perfusion with FITC-dextran and IB4 staining to measure CNV areas. **(A)** CNV areas with FITC-dextran and IB4 staining were captured by fluorescence microscope in non-treatment and RBZ treatment groups. **(B)** CNV areas with FITC-dextran and IB4 staining were captured by fluorescence microscope in CBC treatment groups. Scale bar: 200 μm. **(C)** CNV areas were quantified via ImageJ software. ***P<0.001.

Abbreviation: NS, no significance.

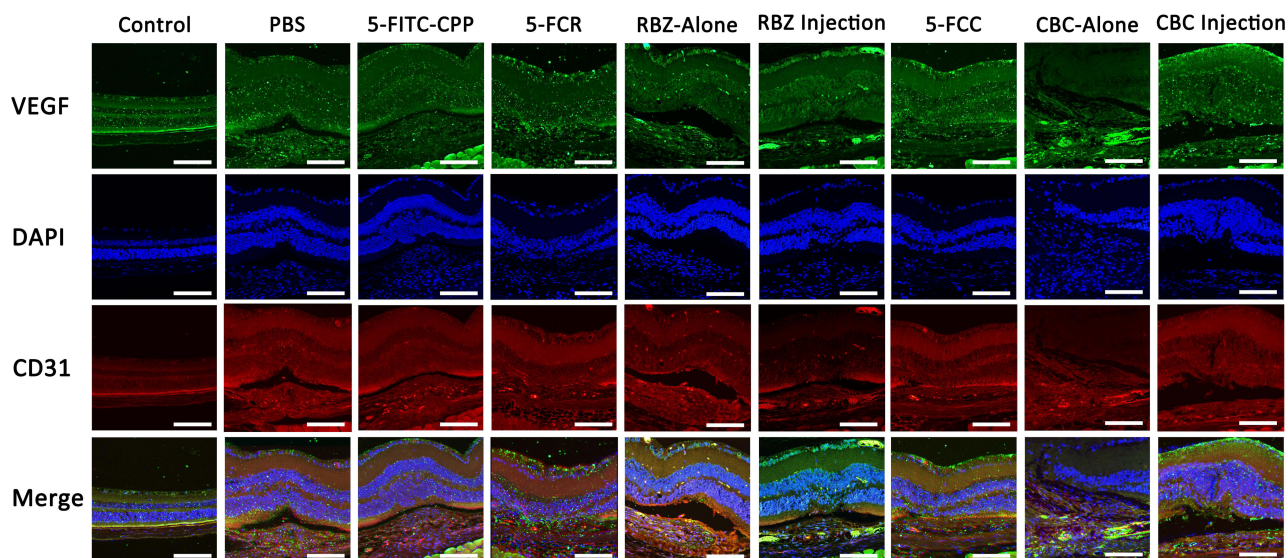


Figure 9 Double immunostainings with endothelial marker CD31 and VEGF in the retina/choroid cryosections were performed in nine groups and images were recorded by fluorescence microscope. Scale bar: 100 μm.

5-FITC-CPP, 5-FCR, and 5-FCC groups, indicating their good biosafety (Figure 10A). Furthermore, HE staining was performed to assess the potential damage of 5-FCR and 5-FCC eye drops on the eyeball and internal organs. The results revealed that the cornea and retina of the control group, the 5-FITC-CPP group, the 5-FCR group, and the 5-FCC group displayed intact structural layers. No apparent loss or disruption of the structural integrity was observed, indicating that the administration of 5-FITC-CPP, 5-FCR, and 5-FCC eye drops did not induce any noticeable toxic side effects on the

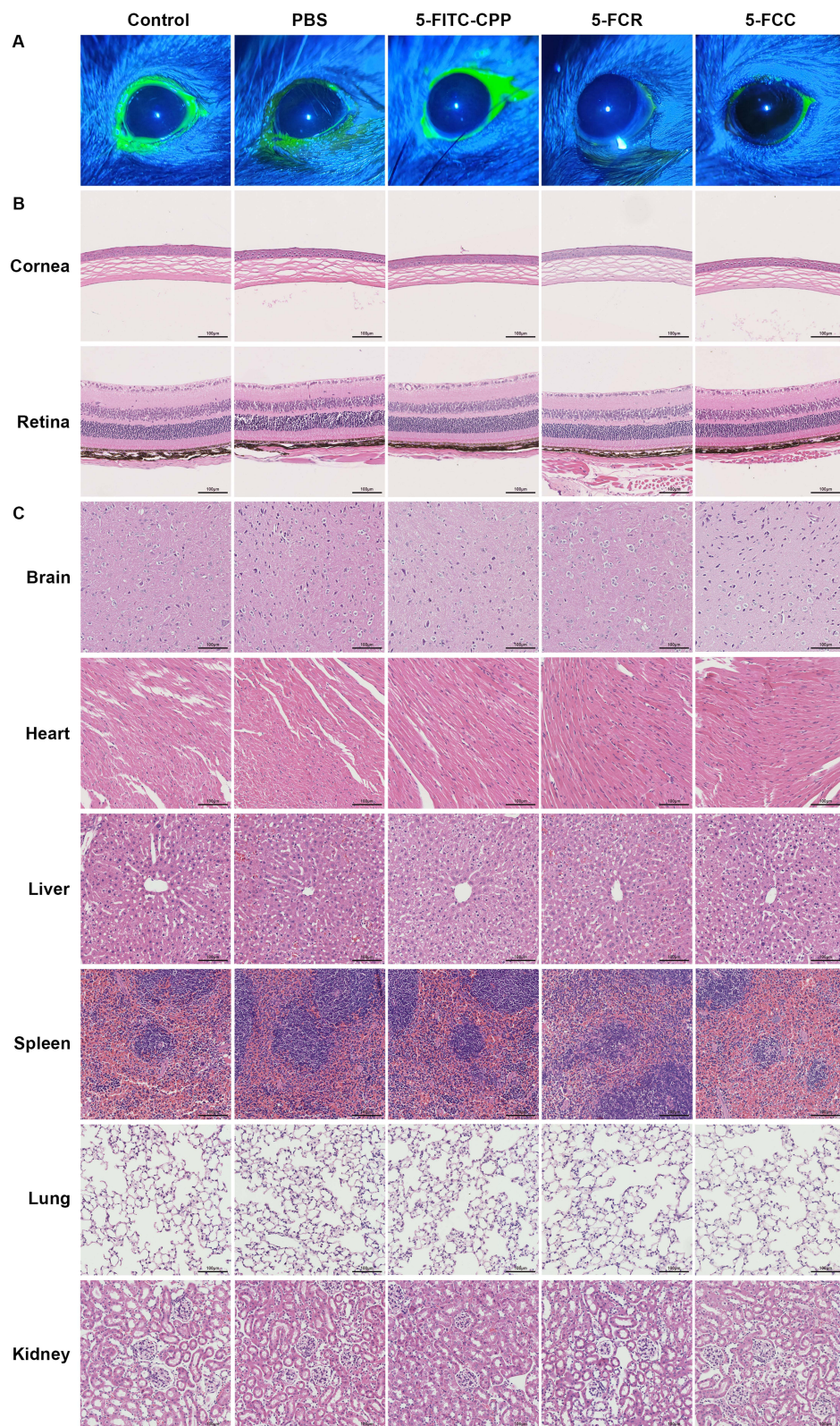


Figure 10 Biosafety analysis of 5-FCR and 5-FCC eye drops. **(A)** Results of fluorescein sodium staining of the cornea of the mice on the 28th day of the intervention. **(B)** Results of HE staining of the cornea and retina. Scale bar: 100 μm. **(C)** Results of HE staining of different internal organ. Scale bar: 100 μm.

cornea and retina of the eye (Figure 10B). Moreover, when compared to the control group, there were no significant alterations in the structure and morphology of the vital internal organs in each experimental group (Figure 10C). Notably, treatment with 5-FITC-CPP, 5-FCR, and 5-FCC eye drops did not cause any substantial organ damage.

Discussion

Previous studies have indicated that CPPs can facilitate the intracellular internalization of hydrophilic biomolecules such as peptides, proteins, and nucleic acids, these cargos can be conjugated to CPPs using covalent bonds or noncovalent complex formation.^{30,31} Current research speculates that complexes predominantly enter cells through endocytic pathways.³² Initially, they bind to negatively charged molecules on the cell surface. Subsequently, a *rac1*-dependent reorganization is triggered, leading to the formation of endocytic vesicles that are engulfed by macrophages. Finally, the peptide penetrates from endocytic vesicles to the cytoplasm, completing the process of cellular internalization. In comparison to other types of delivery vehicles, CPPs exhibit a superior intracellular internalization mechanism without compromising the membrane stability and cellular integrity of target cells.³³ Therefore, CPPs represent a class of excellent drug transport carriers.

In this study, we used arginine as the raw material and obtained the target carrier 5-FITC-CPP through multiple reaction steps. By utilizing the simple charge interaction between CPP and anti-VEGF drugs to non-covalently bind them, we successfully synthesized two eye drop formulations, 5-FCR and 5-FCC, and characterized them through various methods.^{34,35} This method not only enhanced the ability of drugs to traverse tissue barriers and enter cells but also ensured the biological effectiveness of the drugs would not be compromised by the permanent attachment of CPP, while overcoming the complications and adverse reactions that still rely on injection platform administration in previous studies.^{36–38}

The potential toxicity of the carrier-drug complexes is a focal point of our investigation. Previous reports utilized CCK-8 cell viability assays to assess the safety of the three at the cellular level.³⁹ We utilized ARPE-19 cells and HUVECs, commonly encountered at CNV lesion sites, to observe the cytotoxicity of 5-FITC-CPP, 5-FCR, and 5-FCC. Post-intervention, there were no significant changes in cell morphology or activity compared to the control group, displaying results similar to those in Vives et al's study.⁴⁰ According to Harbour et al's research, intervention with penetrating peptides in four different tumor cell lines, even at concentrations as high as 300 μ M, did not induce in significant cell damage.⁴¹

Eye drop solutions must traverse various anatomical regions of the eyeball, ensuring their components do not harm different eye tissues.⁴² In addition, drugs can be metabolized throughout the body through the bloodstream, and it is essential to verify the integrity of various organ structures.⁴³ Through fluorescein sodium staining of the mice corneas,⁴⁴ HE staining of mice eyes, and vital organs, we demonstrated that the three eye drop formulations have excellent biocompatibility at the cellular, tissue, and organ levels, providing assurance for the biological application of eye drops.

VEGF is a potent inducer of CNV, playing a crucial role in promoting neovascularization.⁴⁵ Typically, HUVECs stimulated by VEGF are widely used as cellular models for neovascularization.^{46,47} Cheng et al's study suggests that VEGF can enhance cell migration and promote tube formation by stimulating endothelial cells, reflecting the progress of neovascularization.⁴⁸ Xu et al reported that inhibiting endothelial cell proliferation and VEGF-mediated migration can effectively reduce the formation of new blood vessels, thereby slowing down the development of CNV.⁴⁹ The previous results indicate that the administration of 5-FCR and 5-FCC effectively attenuated VEGF-induced cell proliferation, migration, and tube formation, providing valuable evidence for further in vivo experiments.

To evaluate the effectiveness of 5-FCR and 5-FCC in treating CNV, we induced a mouse CNV model through laser photocoagulation. Currently, methods for constructing CNV animal models include surgical induction, laser photocoagulation, and transgenic approaches.⁵⁰ Laser photocoagulation induction offers advantages such as simplicity, minimal disruption to ocular surface structures, lower cost, and a high success rate.⁵¹ In the laser photocoagulation-induced mouse CNV model, an increase in VEGF expression at the injury site has been reported, which is consistent with a key factor in the development of human CNV, making it a widely used CNV animal model.⁵²

RBZ and CBC are frontline anti-VEGF drugs approved for clinical use, with proven clinical efficacy. Joachim et al's study demonstrated that intravitreal injection of ranibizumab significantly inhibited the progression of laser-induced mouse CNV.⁵³ Du et al successfully lowered vascular endothelial growth factor levels in the eyes of diabetic mice

through intravitreal injection of conbercept.⁵⁴ The series of results in the previous sections indicate that our study successfully delivered RBZ and CBC to the lesions via eye drops, achieving therapeutic effects similar to those observed in the aforementioned studies. Through the downregulation of VEGF expression, the occurrence and development of CNV were effectively suppressed.⁵⁵

Our study established a drug delivery system utilizing cell-penetrating peptides as carriers. The non-invasive drug delivery approach provides a novel option for treating CNV. In comparison to intravitreal drug injections, the use of eye drops significantly enhances patient compliance, reduces associated risks and medical costs. Additionally, the construction of the CPP-drug complex may present a fresh perspective for the treatment of other retinal diseases.

Conclusions

In this study, we have demonstrated a novel drug delivery platform suitable for localized ocular administration. This platform has a broad applicability and does not require chemical linkage with drugs. The results above substantiate that 5-FITC-CPP can safely penetrate the biological barriers in the eye, delivering anti-VEGF drugs to the retinal lesions. Moreover, it has achieved therapeutic efficacy equivalent to intravitreal drug injections. In the future, if this technology progresses to clinical application, it holds promise for bringing substantial benefits to patients with retinal diseases.

Acknowledgments

This study was supported by the Youth Program of National Natural Science Foundation of China (No. 82101130), the Shanghai Natural Science Foundation (No.19ZR1439500), the Ningbo Public Welfare Project (No. 2019C50051), and the Zhejiang Medical and Health Research Project (No. 2019KY643).

Author Contributions

All authors made a significant contribution to the work reported, whether that is in the conception, study design, execution, acquisition of data, analysis and interpretation, or in all these areas; took part in drafting, revising or critically reviewing the article; gave final approval of the version to be published; have agreed on the journal to which the article has been submitted; and agree to be accountable for all aspects of the work. Weinan Hu and Wenting Cai are Co-first authors.

Disclosure

There are no conflicts of interest to declare.

References

1. Folgar FA, Yuan EL, Sevilla MB, et al. Drusen volume and retinal pigment epithelium abnormal thinning volume predict 2-year progression of age-related macular degeneration. *Ophthalmology*. 2016;123:39–50.e1. doi:10.1016/j.ophtha.2015.09.016
2. Thomas CN, Sim DA, Lee WH, et al. Emerging therapies and their delivery for treating age-related macular degeneration. *Br J Pharmacol*. 2022;179(9):1908–1937. doi:10.1111/bph.15459
3. Keenan TDL, Chakravarthy U, Loewenstein A, et al. Automated quantitative assessment of retinal fluid volumes as important biomarkers in neovascular age-related macular degeneration. *Am J Ophthalmol*. 2021;224:267–281. doi:10.1016/j.ajo.2020.12.012
4. Sharma A, Parachuri N, Kumar N, et al. Notion of tolerating subretinal fluid in neovascular AMD: understanding the fine print before the injection pause. *Br J Ophthalmol*. 2021;105(2):149–150. doi:10.1136/bjophthalmol-2020-317933
5. Finn AP, Pistilli M, Tai V, et al. Localized optical coherence tomography precursors of macular atrophy and fibrotic scar in the comparison of age-related macular degeneration treatments trials. *Am J Ophthalmol*. 2021;223:338–347. doi:10.1016/j.ajo.2020.11.002
6. Lai PX, Chen CW, Wei SC, et al. Ultrastrong trapping of VEGF by graphene oxide: anti-angiogenesis application. *Biomaterials*. 2016;109:12–22. doi:10.1016/j.biomaterials.2016.09.005
7. Churm R, Duseath GJ, Prior SL, et al. Development and characterization of an in vitro system of the human retina using cultured cell lines. *Clin Exp Ophthalmol*. 2019;47(8):1055–1062. doi:10.1111/ceo.13578
8. Ishibashi T, Hata Y, Yoshikawa H, et al. Expression of vascular endothelial growth factor in experimental choroidal neovascularization. *Graefes Arch Clin Exp Ophthalmol*. 1997;235(3):159–167. doi:10.1007/BF00941723
9. Ao L, Gao H, Jia L, et al. Matrine inhibits synovial angiogenesis in collagen-induced arthritis rats by regulating HIF-VEGF-Ang and inhibiting the PI3K/Akt signaling pathway. *Mol Immunol*. 2022;141:13–20. doi:10.1016/j.molimm.2021.11.002
10. Xiao Y, Thakkar KN, Zhao H, et al. The m6A RNA demethylase FTO is a HIF-independent synthetic lethal partner with the VHL tumor suppressor. *Proc Natl Acad Sci U S A*. 2020;117(35):21441–21449. doi:10.1073/pnas.2000516117

11. Sarkar A, Junnuthula V, Dyawanapelly S. Ocular therapeutics and molecular delivery strategies for Neovascular Age-Related Macular Degeneration (nAMD). *Int J Mol Sci.* 2021;22. doi:10.3390/ijms221910594
12. Hashida N, Nishida K. Recent advances and future prospects: current status and challenges of the intraocular injection of drugs for vitreoretinal diseases. *Adv Drug Deliv Rev.* 2023;198:114870. doi:10.1016/j.addr.2023.114870
13. Study Investigators IVAN, Chakravarthy U, Harding SP, et al. Ranibizumab versus bevacizumab to treat neovascular age-related macular degeneration: one-year findings from the IVAN randomized trial. *Ophthalmology.* 2012;119(7):1399–1411. doi:10.1016/j.ophtha.2012.04.015
14. Li X, Xu G, Wang Y, et al. Safety and efficacy of conbercept in neovascular age-related macular degeneration: results from a 12-month randomized Phase 2 study: aurora study. *Ophthalmology.* 2014;121(9):1740–1747. doi:10.1016/j.ophtha.2014.03.026
15. Menke MN, Ebnetter A, Zinkernagel MS, Wolf S. Differentiation between good and low-responders to intravitreal ranibizumab for macular edema secondary to retinal vein occlusion. *J Ophthalmol.* 2016;2016:9875741. doi:10.1155/2016/9875741
16. Wei Q, Wan Z, Hu Y, Peng Q. Cytokine and chemokine profile changes in patients after intravitreal conbercept injection for diabetic macular edema. *Drug Des Devel Ther.* 2019;13:4367–4374. doi:10.2147/DDDT.S222004
17. Scondotto G, Crisafulli S, Antonazzo IC, et al. Assessing intravitreal anti-VEGF drug safety using real-world data: methodological challenges in observational research. *Expert Opin Drug Saf.* 2022;21(2):205–214. doi:10.1080/14740338.2021.1957829
18. Cutroneo PM, Giardina C, Ientile V, et al. Overview of the safety of anti-VEGF drugs: analysis of the Italian spontaneous reporting system. *Drug Saf.* 2017;40(11):1131–1140. doi:10.1007/s40264-017-0553-y
19. Ng DS, Ho M, Lu LP, Lai TY. Safety review of anti-VEGF therapy in patients with myopic choroidal neovascularization. *Expert Opin Drug Saf.* 2022;21(1):43–54. doi:10.1080/14740338.2021.1952979
20. Arevalo JF, Sanchez JG, Fromow-Guerra J, et al. Comparison of two doses of primary intravitreal bevacizumab (Avastin) for diffuse diabetic macular edema: results from the Pan-American Collaborative Retina Study Group (PACORES) at 12-month follow-up. *Graefes Arch Clin Exp Ophthalmol.* 2009;247(6):735–743. doi:10.1007/s00417-008-1034-x
21. Storey PP, Pancholy M, Wibbelsman TD, et al. Rhegmatogenous Retinal Detachment after Intravitreal Injection of Anti-Vascular Endothelial Growth Factor. *Ophthalmology.* 2019;126(10):1424–1431. doi:10.1016/j.ophtha.2019.04.037
22. Ji K, Zhang Q, Tian M, Xing Y. Comparison of dexamethasone intravitreal implant with intravitreal anti-VEGF injections for the treatment of macular edema secondary to branch retinal vein occlusion: a meta-analysis. *Medicine.* 2019;98(22):e15798. doi:10.1097/MD.00000000000015798
23. Nguyen DD, Luo LJ, Lai JY. Thermogels containing sulfated hyaluronan as novel topical therapeutics for treatment of ocular surface inflammation. *Mater Today Bio.* 2022;13:100183. doi:10.1016/j.mtbio.2021.100183
24. Nguyen DD, Yao CH, Lue SJ, et al. Amination-mediated nano eye-drops with enhanced corneal permeability and effective burst release for acute glaucoma treatment. *Chem Eng J Adv.* 2023;451:138620. doi:10.1016/j.cej.2022.138620
25. Lai JY, Luo LJ, Nguyen DD. Multifunctional glutathione-dependent hydrogel eye drops with enhanced drug bioavailability for glaucoma therapy. *Chem Eng J Adv.* 2020;402:126190. doi:10.1016/j.cej.2020.126190
26. Koo EH, Eghrari AO, Dzhaber D, et al. Presence of SARS-CoV-2 Viral RNA in aqueous humor of asymptomatic individuals. *Am J Ophthalmol.* 2021;230:151–155. doi:10.1016/j.ajo.2021.05.008
27. Gallo M, Defaus S, Andreu D. 1988–2018: thirty years of drug smuggling at the nano scale. Challenges and opportunities of cell-penetrating peptides in biomedical research. *Arch Biochem Biophys.* 2019;661:74–86. doi:10.1016/j.abb.2018.11.010
28. Singh T, Murthy ASN, Yang HJ, et al. Versatility of cell-penetrating peptides for intracellular delivery of siRNA. *Drug Deliv.* 2018;25(1):1996–2006. doi:10.1080/10717544.2018.1543366
29. Porosk L, Gaidutšik I, Langel Ü. Approaches for the discovery of new cell-penetrating peptides. *Expert Opin Drug Discov.* 2021;16:553–565. doi:10.1080/17460441.2021.1851187
30. Guidotti G, Brambilla L, Rossi D. Cell-penetrating peptides: from basic research to clinics. *Trends Pharmacol Sci.* 2017;38(4):406–424. doi:10.1016/j.tips.2017.01.003
31. Yang CJ, Nguyen DD, Lai JY. Poly(l-Histidine)-Mediate on-demand therapeutic delivery of roughened ceria nanocages for treatment of chemical eye injury. *Adv Sci.* 2023;10(26):e2302174. doi:10.1002/advs.202302174
32. Palm-Apergi C, Lonn P, Dowdy SF. Do cell-penetrating peptides actually “penetrate” cellular membranes? *Mol Ther.* 2012;20(4):695–697. doi:10.1038/mt.2012.40
33. Lonn P, Kacsinta AD, Cui X-S, et al. Enhancing endosomal escape for intracellular delivery of macromolecular biologic therapeutics. *Sci Rep.* 2016;6(1):32301. doi:10.1038/srep32301
34. Siddique AB, Amr D, Abbas A, et al. Synthesis of hydroxyethylcellulose phthalate-modified silver nanoparticles and their multifunctional applications as an efficient antibacterial, photocatalytic and mercury-selective sensing agent. *Int J Biol Macromol.* 2023;256:128009. doi:10.1016/j.ijbiomac.2023.128009
35. Lipok M, Obstarczyk P, Žak A, et al. Single gold nanobipyramids sensing the chirality of amyloids. *J Phys Chem Lett.* 2023;14(49):11084–11091. doi:10.1021/acs.jpcclett.3c02762
36. Wang Y, Lin H, Lin S, et al. Cell-penetrating peptide TAT-mediated delivery of acidic FGF to retina and protection against ischemia-reperfusion injury in rats. *Cell Mol Med.* 2010;14(7):1998–2005. doi:10.1111/j.1582-4934.2009.00786.x
37. Anand A, Jian HJ, Huang HH, et al. Anti-angiogenic carbon nanovesicles loaded with bevacizumab for the treatment of age-related macular degeneration. *Carbon.* 2023;201:362–370. doi:10.1016/j.carbon.2022.09.045
38. Luo LJ, Jian HJ, Harroun SG, et al. Targeting nanocomposites with anti-oxidative/inflammatory/angiogenic activities for synergistically alleviating macular degeneration. *Appl Mater Today.* 2021;24:101156. doi:10.1016/j.apmt.2021.101156
39. Bai N, Hou DQ, Mao CP, et al. MiR-376c-3p targets heparin-binding EGF-like growth factor (HBEGF) to inhibit proliferation and invasion in medullary thyroid carcinoma cells. *Arch Med Sci.* 2020;16(4):878–887. doi:10.5114/aoms.2019.85244
40. Vivès E, Brodin P, Lebleu B. A truncated HIV-1 Tat protein basic domain rapidly translocates through the plasma membrane and accumulates in the cell nucleus. *J Biol Chem.* 1997;272:16010–16017. doi:10.1074/jbc.272.25.16010
41. Harbour JW, Worley L, Ma D, et al. Transducible peptide therapy for uveal melanoma and retinoblastoma. *Arch Ophthalmol.* 2002;120(10):1341–1346. doi:10.1001/archophth.120.10.1341
42. Abullatif AM, Hassan LM, Shash RY, et al. Safety and efficacy of black tea extract in the treatment of acute bacterial conjunctivitis: a rabbit model. *Eye Contact Lens.* 2023;49(1):35–41. doi:10.1097/ICL.0000000000000954

43. Kim J, Kim ED, Shin HS, et al. Effectiveness and safety of injectable human papilloma virus vaccine administered as eyedrops. *Vaccine*. 2023;41(1):92–100. doi:10.1016/j.vaccine.2022.09.070
44. Singh A, Cho WKJ, Pulimamidi VK, et al. Interleukin-11 suppresses ocular surface inflammation and accelerates wound healing. *Invest Ophthalmol Vis Sci*. 2023;64:1. doi:10.1167/iovs.64.14.1
45. Nguyen DD, Luo LJ, Yang CJ, et al. Highly retina-permeating and long-acting resveratrol/metformin nanotherapeutics for enhanced treatment of macular degeneration. *ACS Nano*. 2023;17(1):168–183. doi:10.1021/acsnano.2c05824
46. Cerezo AB, Hornedo-Ortega R, Álvarez-Fernández MA, et al. Inhibition of VEGF-induced VEGFR-2 activation and HUVEC migration by melatonin and other bioactive indolic compounds. *Nutrients*. 2017;9(3):E249. doi:10.3390/nu9030249
47. Park SL, Won SY, Song JH, et al. Esculetin inhibits VEGF-induced angiogenesis both in vitro and in vivo. *Am J Chin Med*. 2016;44(01):61–76. doi:10.1142/S0192415X1650004X
48. Cheng H, Zhao Y, Wang Y, et al. The potential of novel synthesized carbon dots derived resveratrol using one-pot green method in accelerating in vivo wound healing. *Int J Nanomed*. 2023;18:6813–6828. doi:10.2147/IJN.S434071
49. Xu L, Wang W, Meng T, et al. New microtubulin inhibitor MT189 suppresses angiogenesis via the JNK-VEGF/VEGFR2 signaling axis. *Cancer Lett*. 2018;416:57–65. doi:10.1016/j.canlet.2017.12.022
50. Grossniklaus HE, Kang SJ, Berglin L. Animal models of choroidal and retinal neovascularization. *Prog Retin Eye Res*. 2010;29(6):500–519. doi:10.1016/j.preteyeres.2010.05.003
51. Hara C, Kasai A, Gomi F, et al. Laser-induced choroidal neovascularization in mice attenuated by deficiency in the apelin-APJ system. *Invest Ophthalmol Vis Sci*. 2013;54(6):4321–4329. doi:10.1167/iovs.13-11611
52. Yamada K, Sakurai E, Itaya M, et al. Inhibition of laser-induced choroidal neovascularization by atorvastatin by downregulation of monocyte chemoattractant protein-1 synthesis in mice. *Invest Ophthalmol Vis Sci*. 2007;48(4):1839–1843. doi:10.1167/iovs.06-1085
53. Joachim SC, Renner M, Reinhard J, et al. Protective effects on the retina after ranibizumab treatment in an ischemia model. *PLoS One*. 2017;12(8):e0182407. doi:10.1371/journal.pone.0182407
54. Du L, Peng H, Wu Q, et al. Observation of total VEGF level in hyperglycemic mouse eyes after intravitreal injection of the novel anti-VEGF drug conbercept. *Mol Vis*. 2015;21:185–193.
55. Zhu H, Ye J, Wu Y, et al. A synergistic therapy with antioxidant and anti-VEGF: towards its safe and effective elimination for corneal neovascularization. *Adv Healthc Mater*. 2023:e2302192. doi:10.1002/adhm.202302192

International Journal of Nanomedicine

Dovepress

Publish your work in this journal

The International Journal of Nanomedicine is an international, peer-reviewed journal focusing on the application of nanotechnology in diagnostics, therapeutics, and drug delivery systems throughout the biomedical field. This journal is indexed on PubMed Central, MedLine, CAS, SciSearch®, Current Contents®/Clinical Medicine, Journal Citation Reports/Science Edition, EMBase, Scopus and the Elsevier Bibliographic databases. The manuscript management system is completely online and includes a very quick and fair peer-review system, which is all easy to use. Visit <http://www.dovepress.com/testimonials.php> to read real quotes from published authors.

Submit your manuscript here: <https://www.dovepress.com/international-journal-of-nanomedicine-journal>